

# HET603 Project

## 100: Deep Field

David Higgins

### ***Abstract***

This paper presents the photometry of galaxies observed in the field containing the Abell 1631 galaxy cluster using broadband photometry (BVRI) and relates the results to the known redshifts,  $z$ , for these galaxies. The results indicate that observed photometric colour indices, broadly speaking, reveal the redshift, or distance, of the observed galaxy. The plot has also indicated the presence of a second cluster of galaxies whose most predominant member is likely NGC 4756 at a distance of some 53 mega parsecs.

### ***Introduction***

For this project I chose the Abell 1631 galaxy cluster. This field is centred on J2000 RA 12 52 46.47 Dec -15 26 14.3. It was chosen for its lack of bright field stars allowing me to image for long periods without causing field objects to bloom and its relative sparseness makes it easier to conduct accurate aperture photometry. The field has a large number and a good range of galaxies including various types of Spirals and ellipticals as well as a good range of stars from almost the entire spectrum ranging from O to M. A chart of the chosen field is shown at Figure 6. The view that this field represents can be described by a Galactic Latitude of 47.5 and a Galactic Longitude of 303 and a Supergalactic Latitude of -4.6 and a Supergalactic Longitude of 131.2.

The Galaxy Cluster has a mean redshift of 0.0508 and is situated some 600 million LY away containing 34 catalogued galaxies. Note that the brightest galaxy located in the centre of this cluster (NGC 4756) is not actually part of the cluster as it lies only 160 million LY distant. The cluster was catalogued by UCLA astronomer George Ogden Abell (1927-1983) in 1958 as part of his PhD Thesis and was based on visual inspection of the red 103a-E photographic plates of the Palomar Sky Survey POSS. This was known as the Northern Survey. A further southern survey to cover the sky south of Dec -27 was completed in 1989 after his death. (Wiki, 2006)

### ***Equipment Setup***

Hunters Hill Observatory is fitted with a Meade 0.36m LX200GPS Schmidt Cassegrain Telescope (SCT) operating at f/4 imaging through a Meade f/3.3 Focal Reducer (FR). Imaging is performed by an SBIG ST-8E CCD camera fitted with a Kodak KAF1602E CCD operating at Bin 2x2. The camera is fitted with an SBIG CFW-8 filter wheel fitted with Schuler BVRI filters meeting the specifications defined by Michael S Bessell.



**Figure 1:** Hunters Hill Observatory interior view

The equipment is permanently setup in a roll top observatory. Telescope and Imaging control is via the observatory PC which is hooked linked to the home LAN via CAT5 cable. The PC operates under Windows 2000 Professional Operating System (Service Pack 4) running ACP4 version 4.1.11 by DC3. ACP4 is the automation package that allows the observatory to run unattended all night. It controls the telescope directly through a Serial interface and the camera via MaxIm DL/CCD version 4.5. The LX200GPS is fitted with a software controllable focusing unit and ACP provides autofocus via a 3<sup>rd</sup> party software called FocusMax. Each image is automatically plate solved via Pinpoint 4 by DC3. The main telescope is guided via a piggybacked 0.1m Meade SCT fitted with a Meade f/6.3 FR and Starlight Xpress MX716 CCD camera.

**Table 1:** SBIG ST-8E CCD Specifications

Number of Pixels	Pixel Size	Array Size	Read Noise	Full Well CapacityType	Notes
1530 x 1020	9 x 9 $\mu$ m	13.9x9.2mm	15e <sup>-</sup> rms	50Ke <sup>-</sup> /100Ke <sup>-</sup>	NABG

**CCD QUANTUM EFFICIENCY**  
(KAF 1602E, used in SBIG ST-8E)

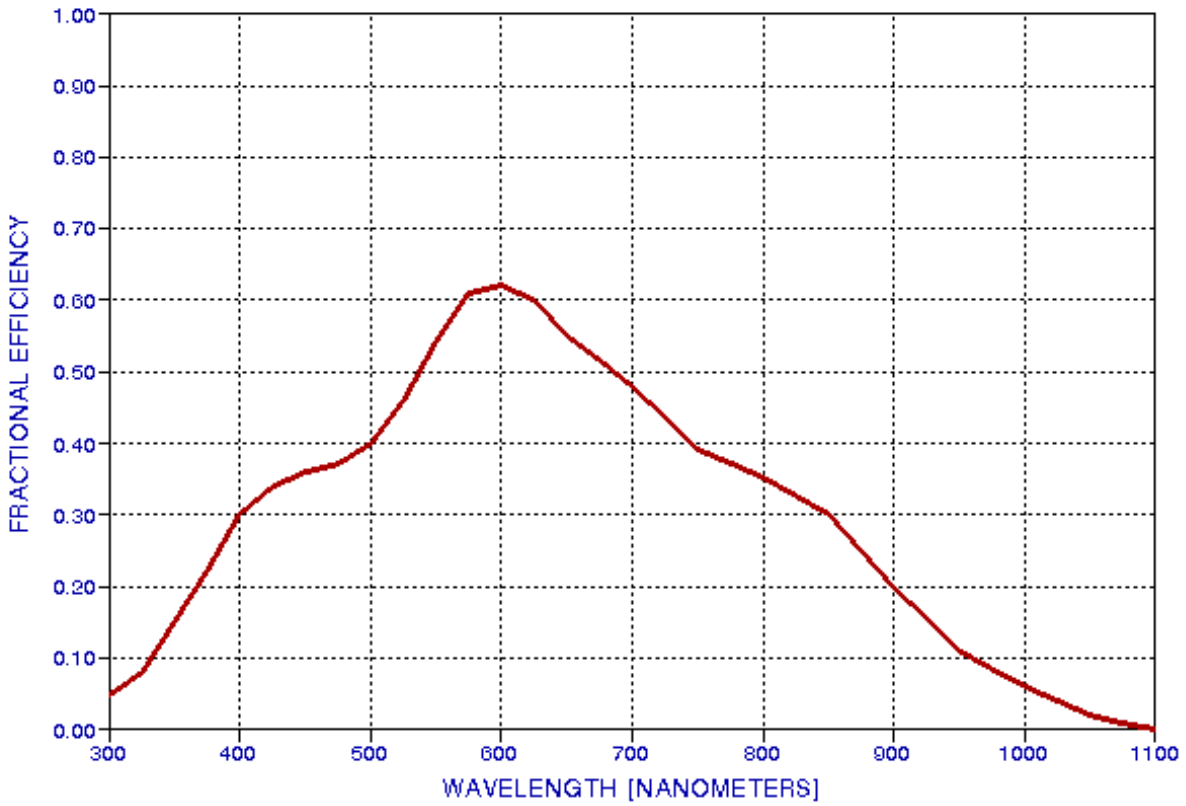


**Figure 2:** QE of the Kodak KAF1602E CCD chip fitted in the SBIG ST-8E

Figure 3 provides the transmission ratings for the Schuler BVRI filters used in the optical train. The QE chart for the KAF1602E chip at figure 2 indicates that the CCD is most sensitive in the R band (62%), somewhat less sensitivity in the V band (47%), I Band (37%) and B band (33%).

On top of this we need to consider the telescope optics itself. Meade has published the following chart for its LX200GPS range of scopes with UHT Coatings. The transmission rating for the Meade LX200GPS with UHTC coatings can be seen in Figure 4.

The coatings allow the following transmission of light in each band: B ~ 80%, V ~ 91%, R ~ 90% and I ~ 78% while the light transmission through each filter are B ~ 75%, V ~ 85%, R ~ 77% and I ~ 77%. Based on the values of transmission through the telescope optics, the filter and CCD QE we can calculate that the system is not as sensitive in the blue so B filter exposures will need to be much longer than the others.

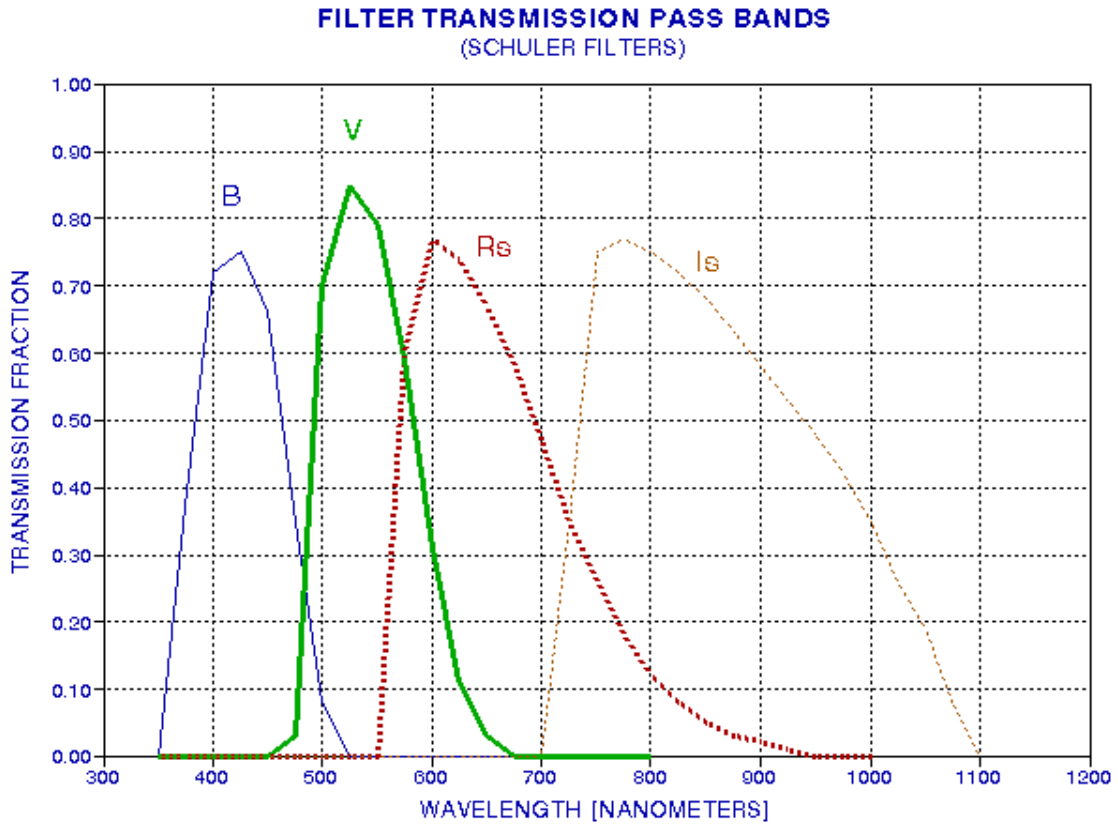


**Figure 3:** Wavelength coverage of Schuler Johnson and Cousins BVRI filters. Peak performance for each filter is indicated. Bj ~ 425nm, Vj ~ 525nm, Rc ~ 600nm and Ic ~ 775nm

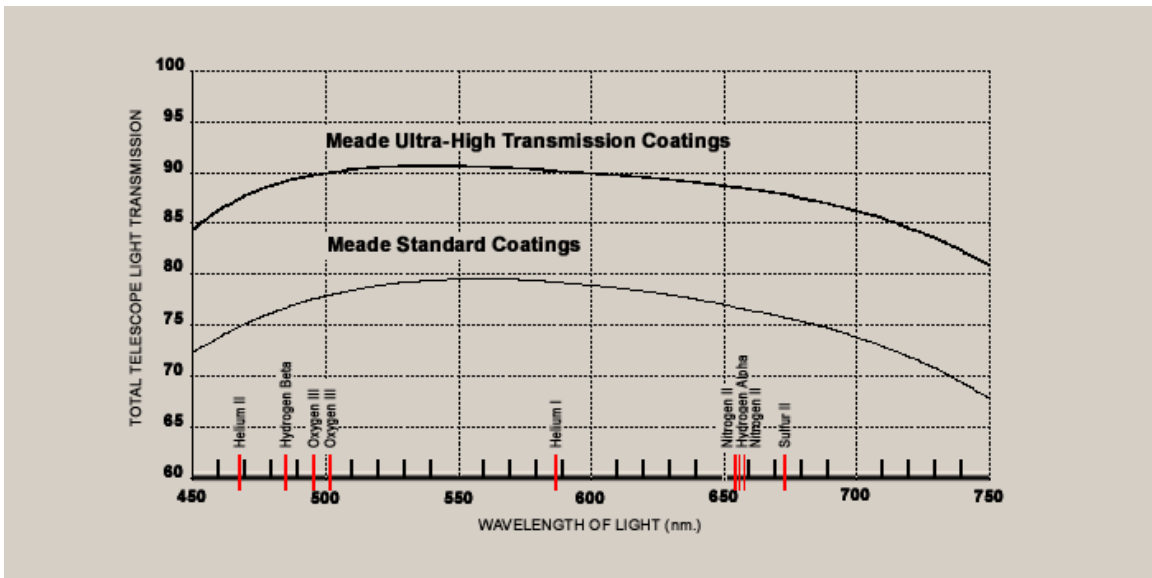


**Figure 4:** Total Telescope Transmission levels

## Method

In April of 2006, images of the ABELL 1631 field were obtained. Over a series of several nights, short integration images in each filter (BVRI) were taken using the exposure times predicted from the light transmission for each colour. All images for each night were co-added using Median Combine using the automated platesolve and track and stack function in Astrometrica after being suitably calibrated with flat and dark frames. The results of each night were then sum combined for each filter in MaxIm DL/CCD. The big advantage of Median Combining each filter was this it removed cosmic ray hits and satellite trails.

Each night a neighboring Landolt star field was imaged to obtain colour transforms. Unfortunately I did not take sufficient images to obtain nightly extinction and zero points. However, I only wanted to obtain colour indexes for each object.

In the end I used MaxIm DL/CCD's colour combine facility to join the B, V, R and I images to form a final colour image shown in Figure 5. This image represents 90 minutes in V, 201 minutes in each of B and I and 109 minutes in R for a total of 10 hours imaging.

## Colour Transforms and Image Calibration

In order to take care of colour variations based on the optical system used the variation between my systems colour sensitivity and that of the standard system was calculated. This is known as Colour Transforms. The method used was to measure a standard field several times in each filter then plot the colour indexes measured against the Standard field measured colour indexes. (These plots can be seen at Appendix A.)

The following colour transforms were calculated based on images taken of the Standard field - Landolt PG1323.

**Table 2: Colour Transforms**

<b><math>B-V = 1.0863 * b-v + 0.0634</math></b>
<b><math>V-R = 1.08705 * v-r + 0.0354</math></b>
<b><math>R-I = 0.9642 * r-i + 0.0088</math></b>

These transforms take the form: Standard = A \* Measured + B

Calibrating from the Landolt Standard field I was able to obtain instrumental magnitudes for each filtered image and chose several comparison stars for the Abell 1631 field. Using these comp stars I was able to measure the instrumental B, V, R and I magnitudes for each object using aperture photometry and obtain the B-V, V-R and R-I colour indices. Although not ideal, I was restricted to a 9 pixel aperture for most targets in order to avoid contamination from neighbouring objects. (A handful required an aperture of 5 pixels). This, of course, means that for some objects the majority of the measured light came from the galactic core where other smaller galaxies had their entire radiation measured.

Once the instrumental values had been measured and the colour indices calculated, the colour transforms contained in Table 2 were applied to obtain the standard indices for each measured object.

**Table 3:** Instrumental Colour Indexes in the Abell 1631 field

Star	iVj	iBj-iVj	iVj-iRc	iRc-iIc
A	11.873	0.467	0.255	0.331
B	12.059	0.849	0.426	0.529
C	12.151	0.631	0.349	0.370
D	13.458	0.737	0.416	0.418
E	13.313	0.537	0.308	0.337
F	14.104	0.593	0.337	0.339
G	12.123	0.781	0.435	0.416

The Instrumental values do not include extinctions or nightly zero points as I am only interested in the colour Indices. Second order for B filter was not considered necessary since the Landolt and Abell 1631 fields are relatively close together.



**Figure 5.** Tri colour image of Abell 1631.  
Letters indicate Comparison stars listed in Table 3  
Copyright David Higgins 2006

The SNR for each measure was used to indicate the error in the indices given by the formula:

$$\text{Err}[\text{Target}] = 1.0857/\text{SNR}[\text{target}] \quad [1]$$

The factor of 1.0857 converts flux to magnitudes (Howell). The figures for Instrumental Bj and Rc are shown in the Catalogue at Appendix B. A couple of galaxies in the field were far too faint in B to obtain any B magnitude and another handful had very low SNR's generating very large errors. They're data, however, has still been included in the plot.

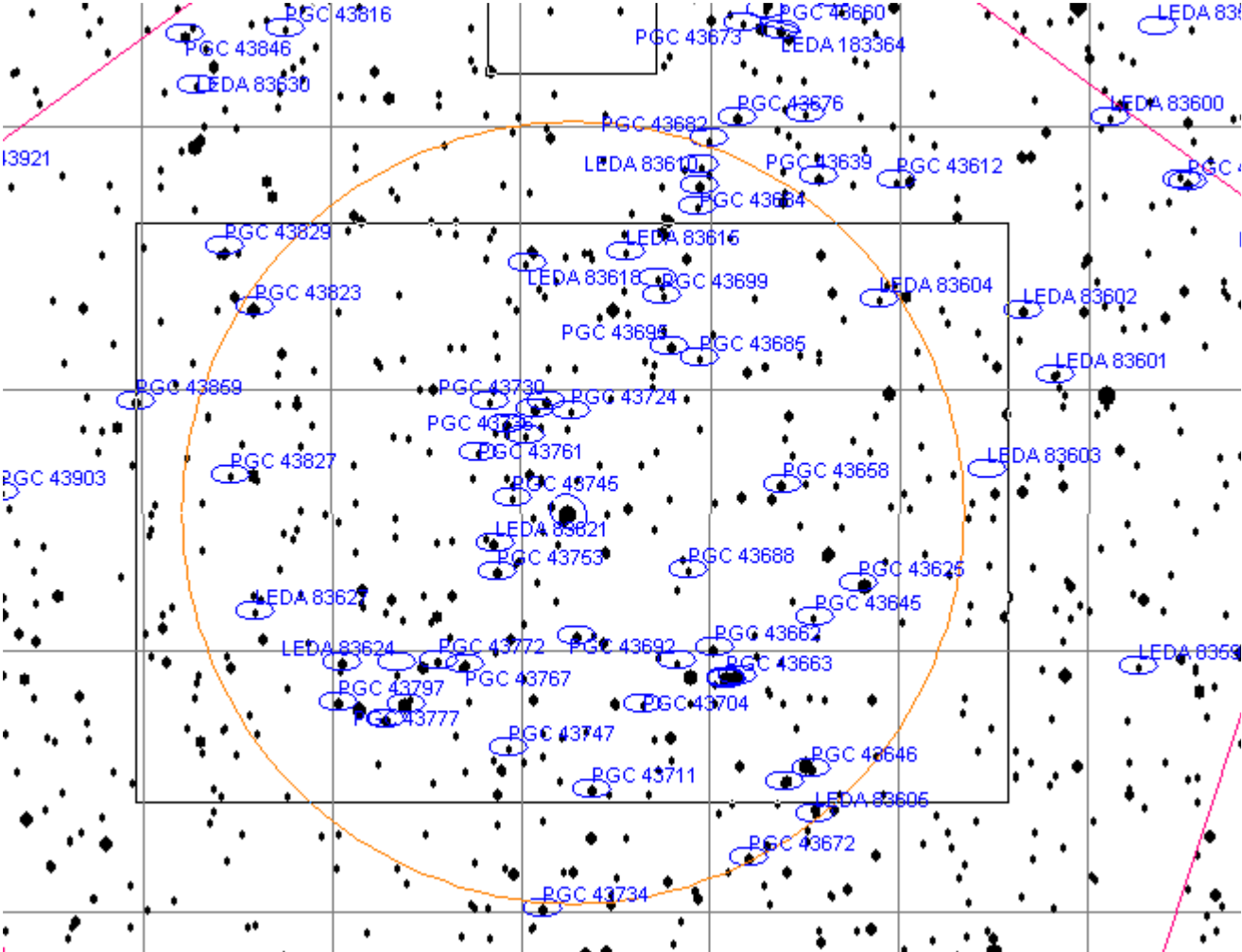


**Figure 6:** Catalogues and Chart of Abell 1631  
(Generated by Guide version 8 by ProjectPluto)

**Results**

Redshift is the measure of how far an objects spectral lines has shift (to the red or blue) based on it's location in the universe in relation to us and, as a result, how fast it is receding from us (Radial Velocity). This redshift is a relationship of the wavelength of the light for an object at rest verses the object in motion. Based on Hubbles law, this redshift is directly proportional to the distance of the object (in megaparsecs for small values of z). As such we have:

$$d = c * z / H_0 \tag{2}$$

For small values of  $z$ ,  $H_0 = 75 \text{ km sec}^{-1} \text{ Mpc}^{-1}$  and  $c$  represents the speed of light of  $299,792.458 \text{ km sec}^{-1}$ . Radial Velocity,  $v$ , is represented by:

$$z = v/c \quad [3]$$

As stated, the redshift is a measure of how far the spectral lines have shifted toward the red or blue. This measure is performed using spectroscopy comparing the wavelength of a spectral line at rest,  $\lambda_0$ , with the one measured,  $\lambda$ :

$$z = (\lambda - \lambda_0) / \lambda_0 \quad [4]$$

But what about broadband photometry, what can we hope to achieve? BVRI filters simply break up the visible light into smaller chunks. What is typically done is to convert the measured magnitude into flux then plotted as low resolution spectral energy distributions (SED's) and the redshift is determined by comparing the SED's to redshifted template galaxy spectra. (Gwyn, 1990) This is far too complex for this project but an even broader method might still apply – colour indices.

The catalogue of Galaxies contained in the Abell 1631 field is provided in Appendix B. This catalogue provides the Instrumental BVRI magnitudes, B-V, V-R, R-I colour indices, and photometric errors. The PGC and SIMBAD catalogues provide distance and/or Radial Velocities for all the galaxies in the field. Some catalogues, however, only provided  $z$ , while others only provided Radial Velocity. I used equations [2] and [3] to convert them all to Radial Velocity.

A plot of the objects Radial Velocity against their Colour index is provided at figure 7. As can be seen there is a striking trend showing a general reddening of the galaxies the higher the Radial Velocity (ie the more distant they are). They also appear to be somewhat brighter in the Ic band the further away they get whilst there is little change in the V and R bands (not plotted).

A linear fit to the plotted data was obtained via Microsoft Excel's standard Trend line fit for each set of B-V and R-I data as follows:

$$B-V_{RV} \text{ (km/sec)} = (B-V_m - 0.8954)/2E-05 \quad [5]$$

$$R-I_{RV} \text{ (km/sec)} = (R-I_m - 0.6279)/3E-06 \quad [6]$$

Obviously the statistical pool in this study is very small which can result in selection errors but larger studies of 'Photometric Redshift' including the SEDs approach have shown that precision as high as +/- 0.1  $z$  is possible (not that I am claiming anywhere near that type of precision here using the simple colour index). Spectroscopic Redshift is considerably more accurate with typical errors of approximately 0.001  $z$ . (Gwyn, 1990) What is evident, however, is that broadband colour indices are a very quick means for gauging a galaxy's distance though prone to considerable error. These errors are due to factors that need to be taken into account given the number of galaxies that vary considerably from this trend line.

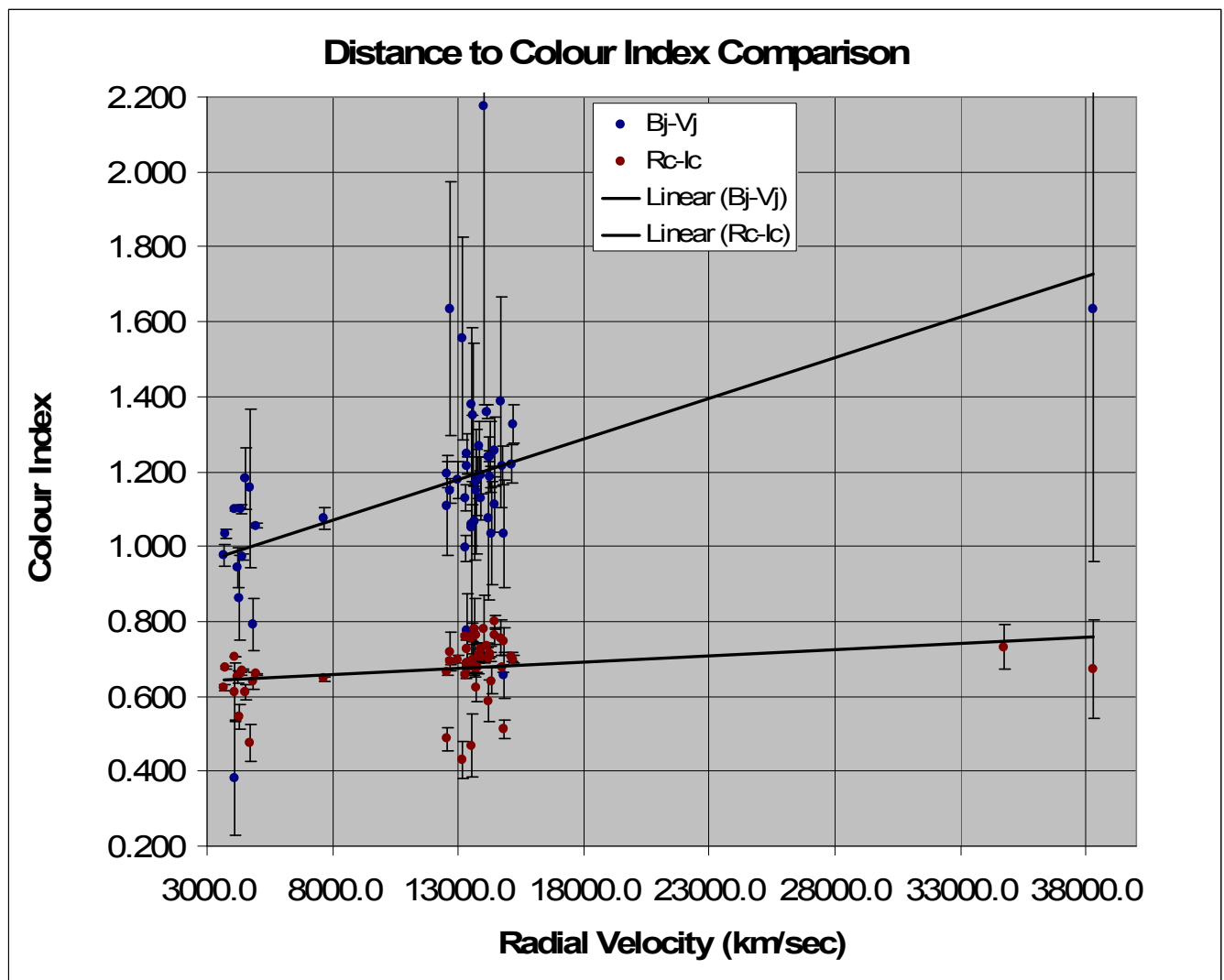


**Figure 7:** Radial Velocity (Distance) to Colour Index Comparison

Other things that can be derived from the plot:

1. There are 2 Galactic clusters in this field. The first is centred on  $150 \times 10^6$  Ly while the actual Abell 1631 cluster is centred around  $590 \times 10^6$  Ly.
2. The more distant the galaxy the fainter it is.
3. The distribution about the linear plot may well have something to do with:
  - a. Type of Galaxy – Ellipticals, Spirals and irregulars
  - b. Age of the Galaxy – This can involve a few things.
    - i. The more distant the galaxy the younger the galaxy that we see appears to be because of light travel time.
    - ii. Galaxies stellar population evolves over time so they can get redder the older they get.
  - c. Radial Velocity – Each galaxy will have its own motion relative to its own group so from our perspective some may be travelling faster or slower than others.

So what can be determined based on the type of galaxy? Galaxies contain 2 parts – the bulge and the disc. Galactic disks generally contain a higher percentage of young population I stars and a low percentage of Old Population I and Population II stars. The Nucleus/Bulge contains a higher percentage of Population II and old population I stars. Young Population I stars are Blue whilst the Older Population II stars are red. Irregular galaxies can be thought of as all disk, Ellipticals as all bulge and Spirals as a median of the 2. This would translate to Bluer, Redder and somewhere in between respectively.

The brightness variation is a pretty big generalisation as the inverse square law applied to brightness is better proof that, for a galaxy of the same luminosity, it gets fainter with distance. The statistical distribution of galactic morphologies from, Universe (7<sup>th</sup> ed):

- 77% Spirals ranging from  $10^8$  to  $2 \times 10^{10} L_{\odot}$  and  $10^9$  to  $4 \times 10^{11} M_{\odot}$
- 20% Ellipticals ranging from  $3 \times 10^5$  to  $10^{11} L_{\odot}$  and  $10^5$  to  $10^{13} M_{\odot}$
- 3% Irregular ranging from  $10^7$  to  $10^9 L_{\odot}$  and  $10^8$  to  $3 \times 10^{10} M_{\odot}$

Indicate that Ellipticals are brighter than Spirals which are brighter than Irregulars for a given mass, however there are large variations in between. Obviously its pointless trying to derive anything from small variations in brightness (derived from the size of the error bars) however, very large variations may mean something. In the Abell 1631 cluster there are 3-4 very bright galaxies observable in the plot indicating that these are perhaps the dominant objects in their cluster, much like Andromeda and the Milky Way dominate the local group. 3 such galaxies can be identified in Abell 1631 and a look at their Luminosity values bares this out. (Statistically there appears to be a strong relationship between Luminosity and Mass)

Now let's consider the age of the galaxies. The redshift difference between the 2 clusters of around  $z = 0.3$  represents an age difference of some 2.4 to 4.7 gigayears. Studies have shown that such periods do result in galactic evolution that will affect the results. Those galaxies that formed directly after the big bang, early type galaxies, get fainter with age whilst late type galaxies appear to show little change. (Gwyn, 1990). The colour evolution of a galaxy obviously depends on its formation epoch compared to the present day and this variation can be calculated but is beyond my capabilities at the present time.

Plotting the known galaxy types on top of this chart reveals that the red end of each cluster is dominated by Elliptical galaxies whilst the blue end contains no Ellipticals at all.

So, what do the faint, very blue ones in this plot indicate? How about the faint and very red? Based on what has already been presented one can speculate that the faint red galaxies are very old and/or small ellipticals while the very faint blue ones are most likely irregulars or small young spiral galaxies.

## **Conclusion**

To read about redshift is one thing but to see it in practise was an eye-opener. I was sceptical that I would be able to do much 'science' with my results. Perhaps like many I had assumed that I needed a Spectroscope to get any valid results for such distant objects. Obviously the 'science' completed in this project is basic and limited in nature but with time and effort the results could be improved by utilising the procedures outlined by Gwyn.

## **References**

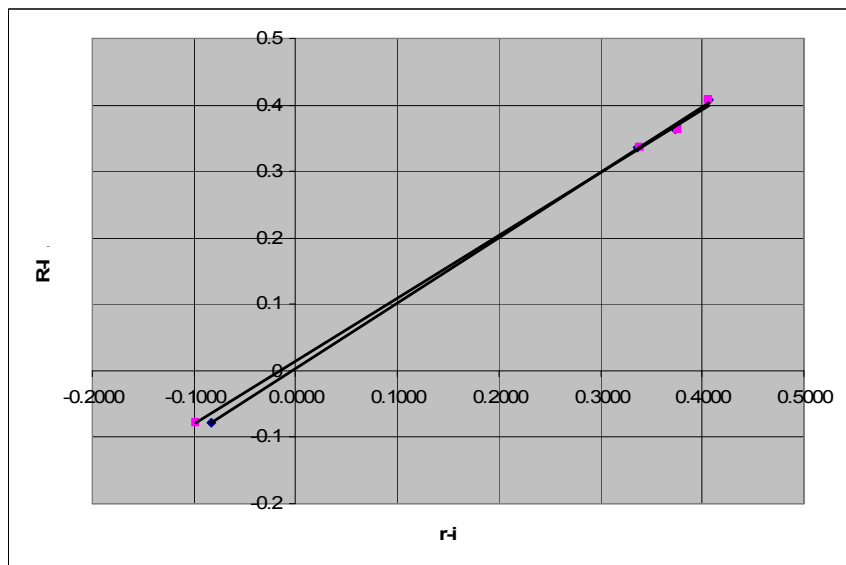
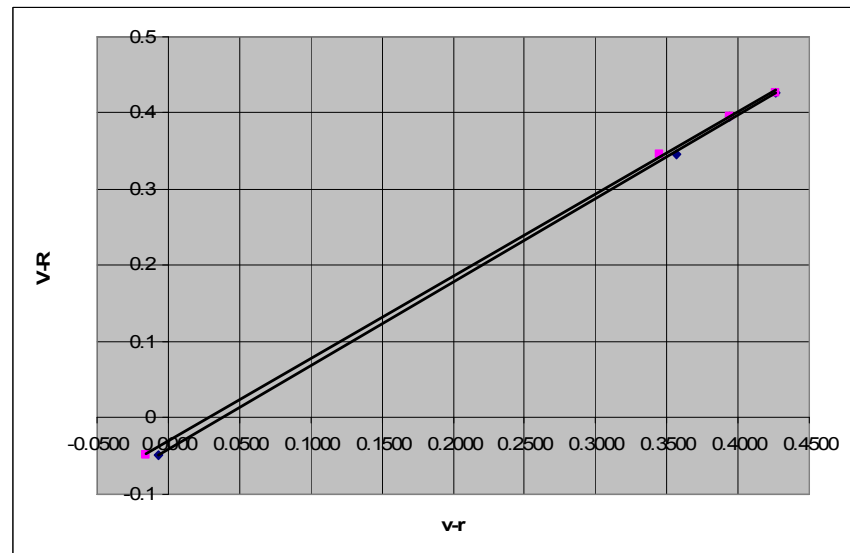
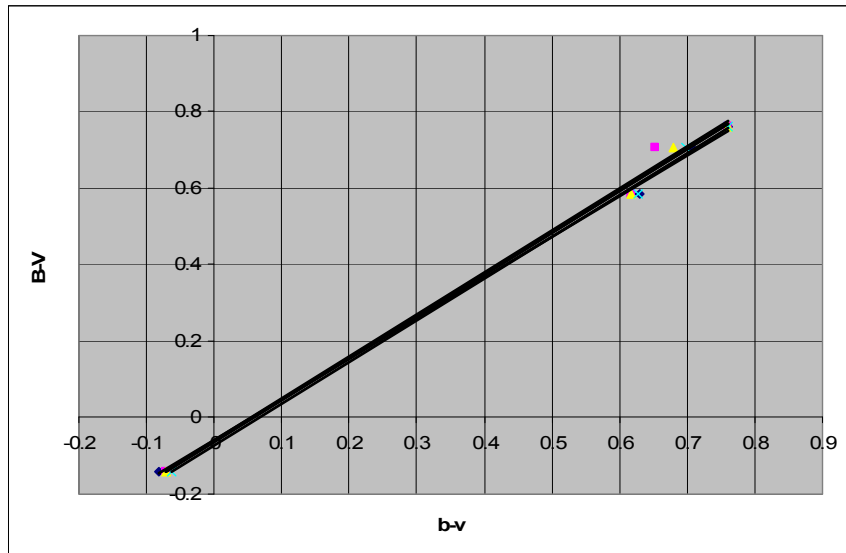
Gwyn, Stephan D.J., 1990: Photometric Redshift of Galaxies. <http://www.astro.uvic.ca/grads/gwyn/pz/>  
Howell, Steven B., Handbook of CCD Astronomy, 2000, p. 57, Cambridge University Press. pp.164.  
ISBN 052164834-3.

PGC Catalogue: LEDA, Observatoire de Lyon, Presented in The Guide by ProjectPluto,  
<http://www.projectpluto.com/datasets.htm#PGC-1996>

SIMBAD: Online reference Database, Centre de Donnees astronomiques de Strasbourg, <http://cdsweb.u-strasbg.fr/>

Wiki, 2006: [http://en.wikipedia.org/wiki/Abell\\_catalogue](http://en.wikipedia.org/wiki/Abell_catalogue)

## Appendix A – Colour Transforms Charts



## Appendix B – Catalogue of Galaxies in the Abell 1631 field imaged at Hunters Hill 2006

Object	J2000 RA	J2000 Dec	ibj	ivj	irc	iic	Actual RV	Err (B)	Err (R)	Bj-Vj	Rc-Ic	Notes
43664	12 52 25.6	S15 31 01.6	15.465	14.571	14.004	13.311	3754.0	0.012	0.003	1.035	0.677	7 x 10 <sup>9</sup> Lum <sub>☉</sub> , Sb
43720	12 52 51.11	S15 29 29.9	16.346	15.506	14.988	14.351	3658.0	0.027	0.008	0.976	0.623	2 x 10 <sup>9</sup> Lum <sub>☉</sub> , Sa
43625	12 52 05.44	S15 27 30.5	15.018	14.180	13.646	12.962	4424.0	0.008	0.002	0.974	0.668	16 x 10 <sup>9</sup> Lum <sub>☉</sub> , Sab
43663	12 52 27.43	S15 31 07.0	14.656	13.743	13.258	12.584	4943.0	0.006	0.001	1.055	0.659	16 x 10 <sup>9</sup> Lum <sub>☉</sub> , E-S0
43662	12 52 29.47	S15 29 58.5	16.389	15.459	14.951	14.290	7637.6	0.029	0.007	1.074	0.646	17 x 10 <sup>9</sup> Lum <sub>☉</sub> , S0-a
43797	12 53 28.95	S15 31 59.7	16.621	15.581	15.030	14.352	12575.0	0.036	0.008	1.193	0.663	19x10 <sup>9</sup> Lum <sub>☉</sub> , S0
43753	12 53 03.84	S15 27 01.7	16.544	15.545	15.003	14.293	12676.0	0.033	0.008	1.149	0.693	17x10 <sup>9</sup> Lum <sub>☉</sub> , E
43685	12 52 31.62	S15 18 50.3	16.935	15.909	15.385	14.670	13003.0	0.048	0.011	1.178	0.698	12 x 10 <sup>9</sup> Lum <sub>☉</sub> , S0
43730	12 52 56.03	S15 20 32.3	16.139	15.079	14.523	13.817	13338.5	0.023	0.005	1.215	0.690	45 x 10 <sup>9</sup> Lum <sub>☉</sub> , E
43736	12 52 57.85	S15 20 49.7	16.394	15.361	14.795	14.067	14289.7	0.029	0.006	1.186	0.711	29 x 10 <sup>9</sup> Lum <sub>☉</sub> , E
43767	12 53 08.99	S15 30 34.8	16.622	15.764	15.226	14.555	13298.0	0.036	0.010	0.995	0.656	19x10 <sup>9</sup> Lum <sub>☉</sub> , S0
43658	12 52 18.57	S15 23 39.8	17.102	16.187	15.596	14.819	13517.1	0.056	0.013	1.057	0.758	13 x 10 <sup>9</sup> Lum <sub>☉</sub> , E-S0
43724	12 52 52.02	S15 20 53.1	17.272	16.162	15.564	14.836	13819.0	0.066	0.013	1.269	0.711	12 x 10 <sup>9</sup> Lum <sub>☉</sub> , S0
43745	12 53 01.47	S15 24 12.8	17.605	16.585	16.085	15.304	13743.0	0.090	0.021	1.171	0.762	8 x 10 <sup>9</sup> Lum <sub>☉</sub> , S0
43761	12 53 06.84	S15 22 28.9	17.081	16.050	15.563	14.872	13809.0	0.055	0.013	1.183	0.675	12 x 10 <sup>9</sup> Lum <sub>☉</sub> , S0
43688	12 52 33.36	S15 26 57.6	17.000	15.963	15.431	14.708	13886.0	0.051	0.012	1.190	0.706	13 x 10 <sup>9</sup> Lum <sub>☉</sub> , E
43772	12 53 13.11	S15 30 27.2	17.182	16.201	15.622	14.877	13893.0	0.060	0.014	1.129	0.727	27x10 <sup>9</sup> Lum <sub>☉</sub> , Sab
43695	12 52 36.28	S15 18 23.3	15.924	14.731	14.758	14.004	14160.0	0.018	0.006	1.359	0.736	31 x 10 <sup>9</sup> Lum <sub>☉</sub> , S0
43777	12 53 18.39	S15 32 04.1	15.694	14.611	14.049	13.329	14201.0	0.015	0.003	1.240	0.703	67x10 <sup>9</sup> Lum <sub>☉</sub> , E-S0
43645	12 52 12.48	S15 28 46.4	17.644	16.548	16.134	15.354	14472.0	0.093	0.022	1.254	0.761	8 x 10 <sup>9</sup> Lum <sub>☉</sub> , S0
43692	12 52 35.21	S15 30 31.6	17.389	16.423	15.872	15.053	14483.0	0.073	0.018	1.113	0.798	15 x 10 <sup>9</sup> Lum <sub>☉</sub> , S0
43704	12 52 40.65	S15 32 06.0	17.041	15.976	15.398	14.676	15146.0	0.053	0.011	1.220	0.705	19 x 10 <sup>9</sup> Lum <sub>☉</sub> , E-S0
43781	12 53 21.55	S15 32 40.4	16.987	15.824	15.273	14.558	15213.0	0.050	0.010	1.327	0.698	28x10 <sup>9</sup> Lum <sub>☉</sub> , S0
43725	12 52 52.57	S15 24 48.0	14.466	13.512	12.964	12.242	4110.6	0.005	0.001	1.100	0.705	E-S0
43675	12 52 33.05	S15 31.01.1	15.458	14.503	13.952	13.277	4376.1	0.012	0.003	1.101	0.660	S0
43748	12 53 02.29	S15 21 21.2	16.616	15.635	15.102	14.326	13309.9	0.035	0.008	1.129	0.757	E-S0
83621	12 53 04.18	S15 25 57.2	17.040	15.949	15.407	14.720	13357.0	0.053	0.011	1.249	0.671	Sab
83622	12 53 04.88	S15 20 32.3	17.055	16.245	15.815	15.149	4224.1	0.053	0.017	0.943	0.651	S0
83624	12 53 19.67	S15 30 54.3	17.640	16.558	16.065	15.333	14289.0	0.093	0.021	1.239	0.715	S0
83625	12 53 28.45	S15 30 29.9	16.979	15.918	15.318	14.627	14766.0	0.050	0.010	1.216	0.675	S0-a
910225	12 53 28.61	S15 30 48.4	18.020	17.057	16.507	16.012	12584.1	0.133	0.032	1.110	0.486	
910409	12 53 04.09	S15 30 03.4	18.059	17.165	16.605	15.950	14307.9	0.138	0.035	1.035	0.640	
910574	12 52 23.07	S15 29 24.6	17.516	16.487	15.976	15.351	4528.1	0.083	0.019	1.181	0.611	
910674	12 52 16.21	S15 28 56.3	19.737	18.291	18.001	17.313	38255.0	0.673	0.131	1.634	0.672	

Object	J2000 RA	J2000 Dec	ibj	ivj	irc	iic	Actual RV	Err (B)	Err (R)	Bj-Vj	Rc-Ic	Notes
910711	12 53 18.93	S15 28 47.9	18.097	17.203	16.699	15.935	14834.0	0.143	0.038	1.035	0.745	
910856	12 52 54.58	S15 28 07.2	17.853	17.117	16.534	15.976	4292.0	0.114	0.033	0.863	0.547	
911011	12 52 57.49	S15 27 24.0	17.349	16.680	16.188	15.532	4824.0	0.071	0.024	0.790	0.641	
911172	12 52 38.18	S15 26 42.1	18.883	17.976	17.542	17.065	13544.0	0.301	0.085	1.049	0.469	
911353	12 52 06.06	S15 25 43.1	18.543	17.613	17.092	16.493	14229.0	0.218	0.055	1.074	0.586	
911411	12 52 56.68	S15 25 25.9	17.720	17.065	16.540	15.798	13354.9	0.100	0.033	0.775	0.724	
911441	12 52 09.21	S15 25 17.5	18.407	17.222	16.769	16.056	13610.0	0.192	0.041	1.351	0.696	
911666	12 52 36.29	S15 24 12.4	19.008	17.561	17.044	16.307	12665.9	0.338	0.053	1.635	0.719	
911807	12 52 56.76	S15 23 33.9	18.779	17.406	17.002	16.565	13195.1	0.272	0.051	1.555	0.430	
911871	12 52 52.29	S15 23 17.1	19.918	17.974	17.605	16.807	14002.1	0.798	0.090	2.175	0.778	
911974	12 52 47.39	S15 22 54.2	17.754	16.831	16.244	15.550	13636.1	0.103	0.025	1.066	0.678	
912260	12 53 04.15	S15 21 38.1	18.813	17.595	16.938	16.163	14730.9	0.281	0.048	1.387	0.756	
912618	12 52 39.15	S15 19 55.4	18.254	17.256	16.758	16.119	13732.9	0.166	0.040	1.148	0.625	
912776	12 52 55.89	S15 19 13.5	18.165	17.874	17.424	16.798	4126.9	0.153	0.076	0.380	0.612	
912855	12 52 12.66	S15 18 53.6	18.483	17.271	16.793	16.021	13534.1	0.206	0.042	1.380	0.753	
3098091	12 52 41.42	S15 30 03.9	18.514	17.508	16.989	16.505	4719.0	0.212	0.050	1.156	0.475	Irregular?
3098092	12 53 11.28	S15 29 30.1	17.202	16.655	16.221	15.699	14833.1	0.061	0.024	0.658	0.512	
910982	12 52 43.52	S15 27 31.1	***	18.092	17.521	16.722	13657.9	***	0.083	***	0.779	
912176	12 52 07.23	S15 21 57.7	***	17.833	17.167	16.419	34701.9	***	0.059	***	0.730	